Available online at www.sciencedirect.com
ScienceDirect
Journal of the European Ceramic Society 26 (2006) 3657–3664
www.elsevier.com/locate/jeurceramsoc

Synthesis and hierarchical pore structure of biomorphic manganese oxide derived from woods

Xufan Li [a], Tongxiang Fan [a,*], Zhaoting Liu [a], Jian Ding [a], Qixin Guo [b], Di Zhang [a]

[a] *State Key Lab of Metal Matrix Composites, Shanghai Jiaotong University, Shanghai 200030, PR China*
[b] *Department of Electronic Engineering, Saga University, Saga 840-8502, Japan*

Received 12 July 2005; received in revised form 14 October 2005; accepted 23 October 2005
Available online 28 December 2005

Abstract

Biomorphic manganese oxides on two different wood templates (fir and paulownia) were fabricated by infiltration with nitrate and subsequently calcination. X-ray diffraction (XRD) test and microscopy observation (FESEM and TEM) were employed to characterize the phase and structure of biomorphic manganese oxides. The pore structure of the resulting products was studied through mercury intrusion and nitrogen adsorption measurement. Infrared (IR) adsorption properties were investigated by Fourier Transmission Infrared (FTIR). The final oxide products contain hierarchical pore structure from μm to nm scale, and also show unique pore size and distribution with hierarchy on nanoscale derived from the specific wood template, the changeable connectivity of nanoscale pore channel controlled by calcinations temperature. The rise of temperature leads to diminishing of average pore diameter and volume but more uniform pore size distribution and higher degree of pore connectivity. The overall collapse in IR adsorption spectra of biomorphic manganese oxides with the rise of calcination temperature is related to the effect of nanoscale pore structure especially the increasing of pore connectivity.

Keywords: Calcination; Porosity; Wood; Manganese; Oxide

1. Introduction

Biological materials, such as wood, bamboo, jute and many others, are characterized by hierarchical architectural design in which organization is controlled with precision on many discrete length scales, ranging from the molecular to the macroscopic.[1,2] Woods[1,3] are natural composites with complex hierarchical cellular structure. They are mainly comprised of biopolymers such as cellulose, hemicellulose and lignin, forming a cellular microstructure of high porosity and interconnectivity. The microstructural features may vary from different kinds of woods: deciduous woods contain tracheas and many other kinds of cell types with various arrangements of them, while coniferous woods possess only a single cell type, the longitudinal tracheids, also known as fibers.

Biomorphic ceramics manufactured by conversion of wood with different infiltration reactions exhibit unidirectional pore structure on micrometer and anisotropic mechanical properties. Examples are carbide ceramics like SiC and SiSiC[4–9,19] and TiC,[10] oxide ceramics like SiO_2,[11] Al_2O_3,[12] TiO_2[13–16] and NiO,[17] ZrO_2,[20] and SiOC/C.[18] However, no report dealt with manganese oxide, which has been reported fabricated as porous materials.[21] And the researches mentioned above focused mainly on the structure within the μm scale, few going deep to the pore structure on nanoscale. The structural hierarchy of wood ranges from mm (growth ring patterns) via μm (tracheidal cell patterns) to nm scale. The nanoscale structure of wood is characterized by the molecular cellulose fiber of cell wall of tracheid or trachea. The cell wall consists of cellulose molecules, which aggregate into microfibrils, and hemicellulose, pectin, glycoprotein and lignin. The composition of cell wall is analogous to a fiber-reinforced organic glass in which cellulose acts as lightweight fiber, lignin as continuous matrix and others as coupling agents.[3,22]

As for the properties and applications of biomorphic materials derived from wood, mechanical properties were widely studied. Researches have proved that the mechanical properties of biomorphic ceramics derived from wood depend on the

* Corresponding author. Tel.: +86 21 62932694; fax: +86 21 62822012.
E-mail address: txfan@sjtu.edu.cn (T. Fan).

0955-2219/$ – see front matter © 2005 Elsevier Ltd. All rights reserved.
doi:10.1016/j.jeurceramsoc.2005.10.015

bulk density and show anisotropy which is largely determined by porosity.[8,12,29] Biomorphic materials with unique pore structure compared to conventionally manufactured porous materials are expected to be of good use in acoustic and heat insulation, filter and catalyst carrier at high temperatures, as well as for medical implant structures,[3,7,8,14,16] and even have electromagnetic shielding properties.[23]

In our research, biomorphic manganese oxides were fabricated on wood templates through a simple synthesis procedure, and the phase formation, pore structure on both micrometer and nanometer scale, and Infrared (IR) adsorption properties are reported.

2. Experimental

2.1. Synthesis

Two kinds of woods fir (classified as coniferous) and paulownia (classified as deciduous) were chosen as the template. They were firstly extracted in boiling 5% weak ammonia for 6 h in order to get rid of the organic acid and lipid, and then washed by distilled water and dried at 80 °C for 1 day. The mixture of 20 mmol $Mn(NO_3)_2$ + 10 ml ethanol + 5 ml H_2O served as the low viscous precursor in which wood templates were immerged at 60 °C for 3 days, making the precursor thoroughly infiltrate into the templates. Then, the infiltrated wood templates were air-dried at 60 °C for 1 day and subsequently calcined at 600, 800 and 1000 °C with heating rate 5 °C/min and holding at peak temperatures for 3 h in electrical heating oven and then naturally cooled to room temperature.

2.2. Characterization

The phases in the biomorphic Mn oxides were identified by means of XRD analysis. A type of JEOL, JDX-3530M diffraction meter using Cu Kα radiation with a Ni filter at 20 kV and 20 mA was employed to obtain a chart recording in the 2θ range from 10° to 90° with scanning step of $0.2^{\circ}s^{-1}$. Field Emission Scanning Electronic Microscopy (FESEM) (FEI SIRION 200) and Transmission Electronic Microscopy (TEM) (Phillip CM-12) were employed to observe the structure and appearance of crystalline grains of biomorphic Mn oxide. The samples were ground into powders and subsequently dispersed in the ethanol for ultrasonic treatment for a few minutes. Several drops of the suspension were then dripped onto a carbon coated copper grid for TEM observation. The pore size distribution on μm scale was detected using mercury intrusion method (AutoPore IV 9500, Micromeritics). Working pressures covered the range from approximately 0.6 to 60,000 psia. The pore size distribution on nm scale was investigated by the nitrogen adsorption measurement and operated on Micromertitics ASAP 2010 adsorption analyzer. The pore size and distribution were measured by BJH method[24] and the pore connectivity was calculated through Seaton's method based on theory of capillary condensation as follows[25,26]:

$$L^{\beta/\gamma}ZF = h[(Zf - 1.5)L^{1/\gamma}] \quad (1)$$

Z is defined for the connectivity of pore network as mean coordination number, expressed as the average number of pores that intersect at a pore junction, while L represents the average linear dimension of pores. Z and L could be calculated simultaneously by fitting the quasi-universal function h of Eq. (1) according to the percolation theory near the percolation threshold. The value of β and γ are 0.88 and 0.41, respectively. f stands for the bond occupation probability, identified as the number of pores which are below their condensation pressure divided by the total number of pores, while the percolation probability, F, is the number of pores from which nitrogen has vaporized, divided by the total number of pores. F and f could be worked out through the results of pore size distribution.

Fourier Transmission Infra-Red (FTIR) (BRUKER EQUINOX 55) was employed for testing the IR adsorption properties of biomorphic Mn oxide. FTIR spectra were recorded with KBr technique and at resolution of $4\,cm^{-1}$. The samples were also ground to powders for nitrogen adsorption and FTIR measurement.

3. Results and discussion

3.1. Phase and pore structure on μm scale analysis

XRD patterns (Fig. 1) indicate that the component of the oxide is mainly Mn_2O_3 at 600 °C, Mn_2O_3 and Mn_3O_4 at 800 °C, and merely Mn_3O_4 at 1000 °C. It is because that $Mn(NO_3)_2$ first decomposed to Mn_2O_3 which converted to Mn_3O_4 beyond 600 °C. Previous research has proved that the decomposition of hemicellulose happens at 190–280 °C, the decomposition of cellulose and lignin happens at 280–500 °C to form amorphous carbon.[27] But the broad peaks of amorphous C do not appear in the pattern because carbon reacted with oxygen released by the decomposition of $Mn(NO_3)_2$ to form carbon dioxide:

$$4Mn(NO_3)_2 \rightarrow 2Mn_2O_3 + 8NO_2 + O_2 \quad (2a)$$

$$6Mn_2O_3 \rightarrow 4Mn_3O_4 + O_2 \quad (2b)$$

$$C + O_2 \rightarrow CO_2 \quad (2c)$$

The skeleton of the porous biomorphic materials is composed of purely Mn oxides. The values of grain size listed in Table 1 were calculated from the full-width at half maximum of the peaks according to the Sherrer equation. With the elevation of calcination temperature, the diffraction peaks become sharper, which results in increasing grain size and more complete crystallization.

The pore arrays of paulownia biomorphic Mn oxide calcined at 600 °C are derived from the unidirectional hollow tracheas growing along axis direction (Fig. 2a). The pores displayed are with diameter range from 8 to 14 μm and round shape which is in accordance with the original pore structure of paulownia. The appearance tangential direction is showed in Fig. 2b. There are also pores distributed on the walls of tracheas accounting for the transportation of liquid substances in the tree. TEM image (Fig. 3) shows that the crystalline grains of fir template biomorphic Mn oxide calcined under 600 °C are nanocrystalline. The

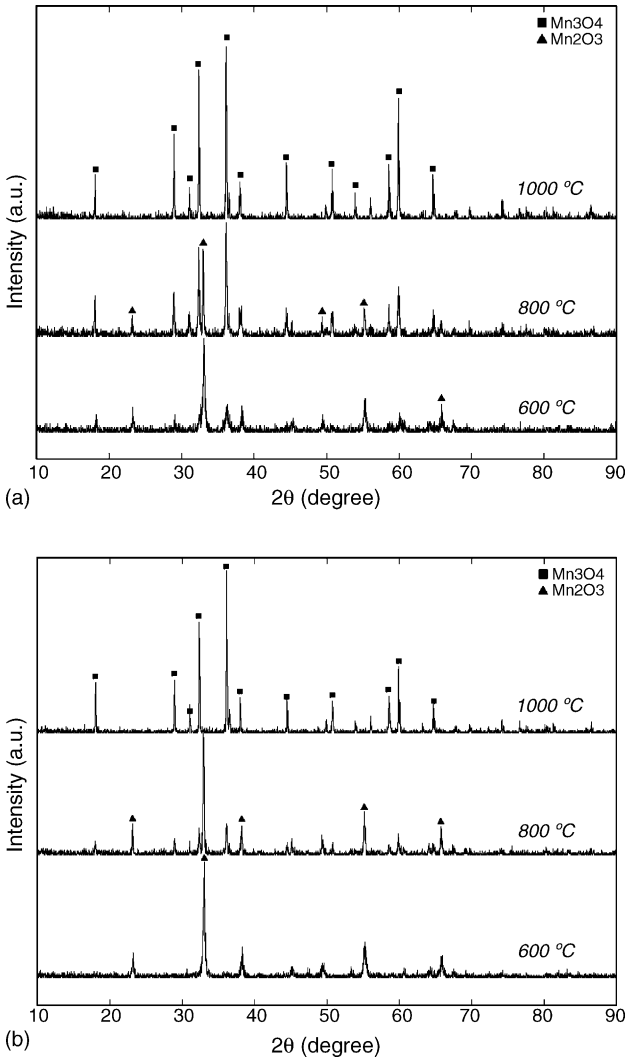

Fig. 1. XRD patterns of biomorphic Mn oxides; (a) fir template; (b) paulownia template.

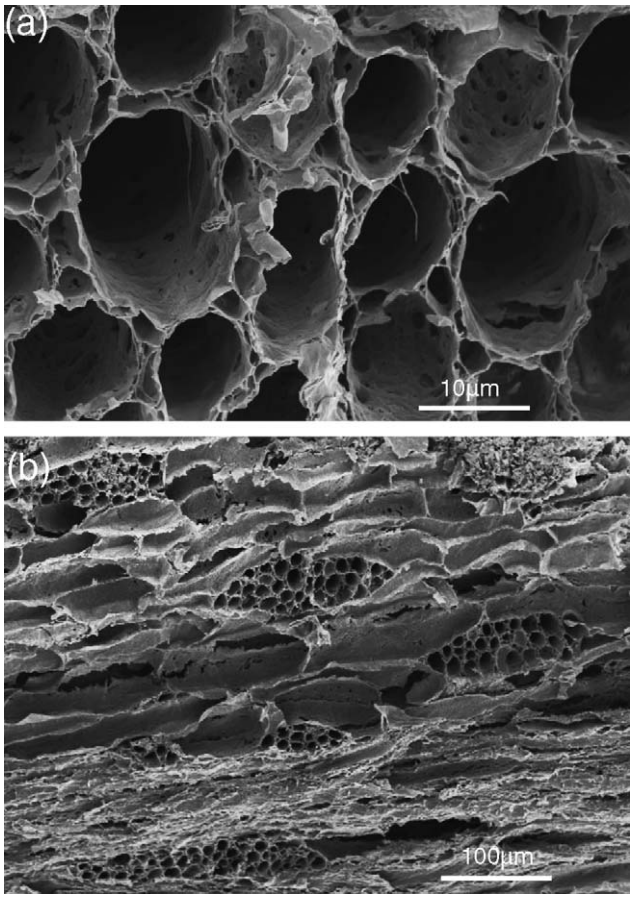

Fig. 2. SEM image of paulownia template biomorphic Mn oxide calcined under 600 °C: (a) cross-section; (b) tangential direction.

diffraction rings denote the isotropy of nanocrystalline grains. Fig. 4 is the TEM image of paulownia template biomorphic Mn oxide calcined under 600 °C. The arrows point at the crystalline grains of Mn_2O_3. The diffraction pattern in Fig. 4c indicates a special texture because the direction of crystal growth was controlled by the unidirectional cellulose arrangement along the longitudinal direction of tree trunk.

The pore sizes are monomodally distributed between 0.1 and 1 μm for fir template product while multimodally distributed between 0.1 and 1 μm, 5 and 50 μm for paulownia template product (Fig. 5) got from mercury intrusion measurement. It is corresponding to the original wood structure. The SEM investigation in Fig. 3a shows that the main pore size of paulownia template biomorphic product is range from 8 to 14 μm. Nevertheless, pore size distribution measured by the mercury intrusion method shown in Fig. 5 indicates that the main pore size range is between 5 and 50 μm. This discrepancy can be explained as that SEM image represents the local character while the results of mercury intrusion method are determined by a general range of pores.

Table 1
Grain size, BET surface area, pore volume and average pore diameter of biomorphic Mn oxides

Template	Calcination temperature (°C)	Grain size (nm)	BET surface area (m^2/g)	Pore volume (cm^3/g)	Average pore diameter (nm)
Fir	600	25.7	21.1	0.1358	10.1
	800	43.2	8.6	0.0184	4.7
	1000	46.3	1.56	0.0024	4.4
Paulownia	600	40.2	24.7	0.1209	8.1
	800	51.5	9.65	0.0231	4.1
	1000	51.9	3.13	0.0027	2.4

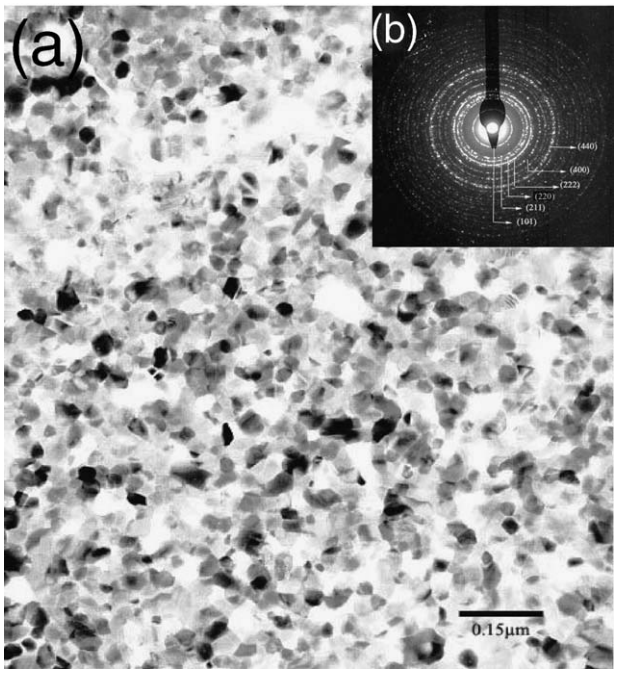

Fig. 3. Crystal grains of biomorphic Mn oxide sintered under 600 °C observed by TEM.

3.2. Pore structure on nanoscale

The nanoscale pores of biomorphic materials derived from wood could be formed by such mechanism.[30] The low viscous liquid precursor penetrated the cell wall, and the following calcination process gave rise to the formation of Mn oxide crystalline grains and the subsequent growth of them with simultaneous removing of elements in cell wall such as cellulose, hemicellulose, lignin, and so on. A continuous matrix of Mn oxide was formed with mesopores left by original wood elements. These mesopores might also be the intercrystalline voids between the oxide grains, or the pinholes in the intergrown oxide layers.[28]

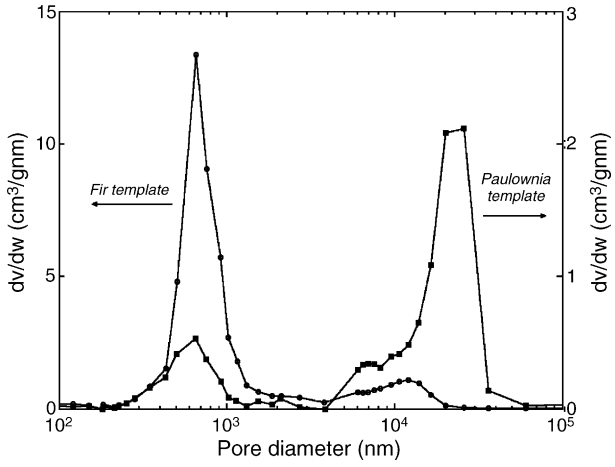

Fig. 5. Pore size distribution from mercury intrusion method of biomorphic Mn oxides calcined under 600 °C.

As the detectable range of mercury is limited within several hundred μm down to several hundred nm, the nanoscale pore structure within the range of meso or micropores should be investigated by nitrogen adsorption measurement.

Figs. 6–8 show, respectively, the N_2 adsorption–desorption isotherms, pore size distribution on nanoscale calculated from the adsorption branch of the isotherms and the outcomes of the fitting process of Eq. (1), from which Z and L were calculated. The results of BET surface area, pore volume and average pore diameter are showed in Table 1.

Under calcination temperature 600 °C, the N_2 adsorption and desorption form hysteresis loops caused by capillary

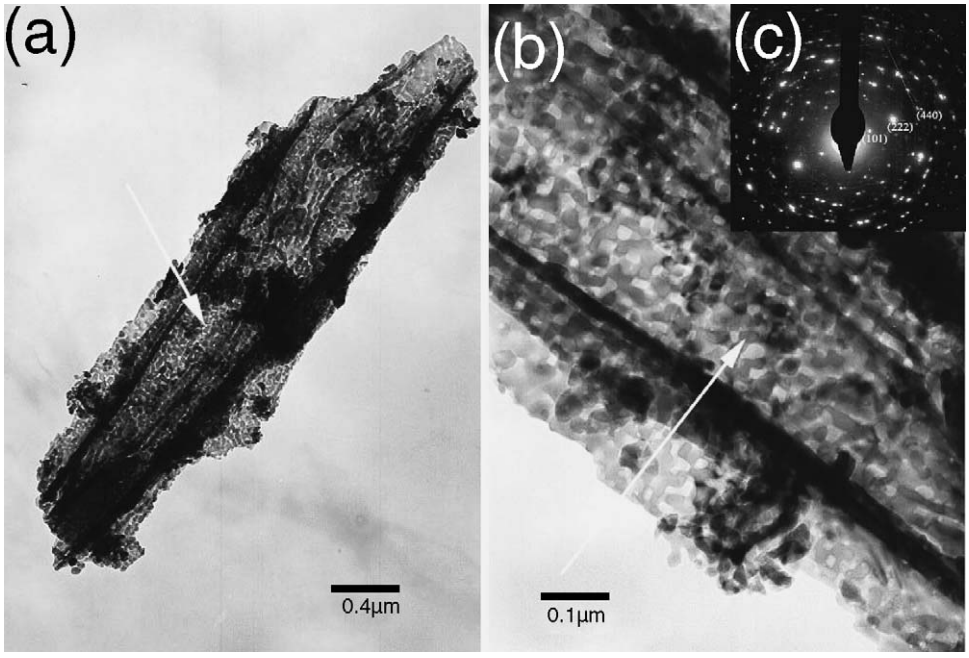

Fig. 4. TEM image of paulownia template biomorphic Mn oxide: (a) 22 k magnification; (b) 75 k magnification.

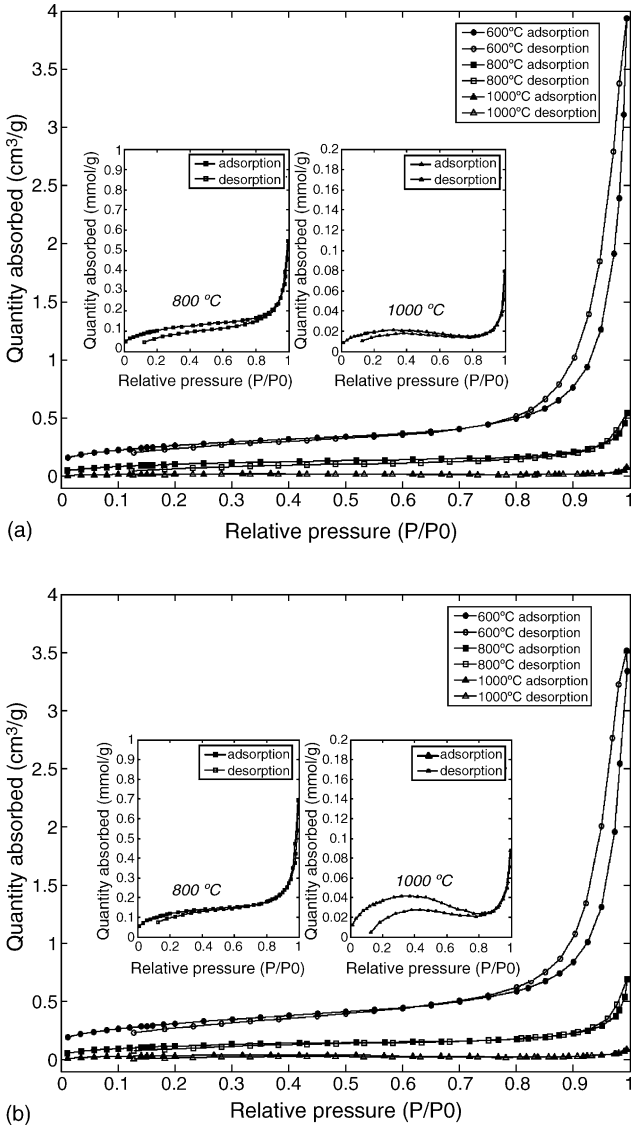

Fig. 6. N_2 adsorption–desorption isotherm of biomorphic Mn oxides: (a) fir template; (b) paulownia tempate.

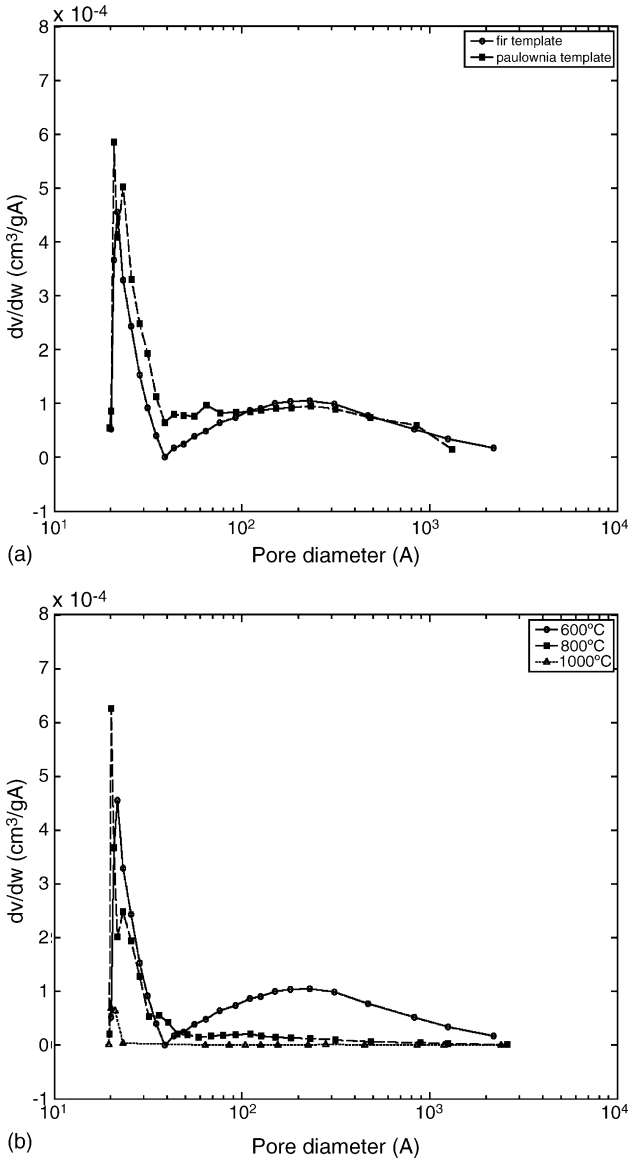

Fig. 7. Pore size distribution of biomorphic Mn oxides: (a) fir and paulownia template sintered under 600 °C; (b) fir template sintered under 600, 800 and 1000 °C.

condensation, exhibiting a *H3*-type of *IV*-type according to IUPAC, which is characteristic of mesoporous solids. *H3*-type isotherm is caused by asymmetric slot-shape pores and channels at mesoscale (pore with size 2–50 nm) that just coincides with wood's pore configuration. With the calcination temperature rising to 800 and 1000 °C, isotherms change almost without hysteresis loops and with less amount of N_2 absorbed. The increase of pore connectivity is attributable to the shrinkage of hysteresis loops on one hand, and on the other hand, the diminishing of pore volume causes less amount of adsorption.

The curves of pore size distribution of biomorphic Mn oxides on both fir and paulownia templates sintered under 600 °C are showed in Fig. 7a. It could be found that the pore size distribution pattern of fir template biomorphic manganese oxide has a sharp peak at 2.2 nm while the pattern of paulownia template one has two peaks at 2.1 and 2.3 nm, and the peak area of fir template ceramic is narrower than that of paulownia template one. Both of the two curves have low broad peaks centered at about 20 nm. On combination of Fig. 7 with the results of Fig. 5 discussed in Section 3.1, it is clearly that the pore structures are hierarchical from μm to nm scale. Moreover, the pores are distributed hierarchically even within the nanoscale with most pores sized around 2.2 nm and some around 20 nm. The discrepancy in pore size distribution between fir and paulownia template biomorphic Mn oxide results from the difference in composition of the molecular cellulose fiber of cell wall of tracheid or trachea in the original woods. Fig. 7b illustrates the influence of sintering temperature on the nanoscale pore size distribution of biomorphic Mn oxides on the same wood template. With the rise of calcination temperature, the sharp peak of pore size distribution curve move backward on X-axis, which

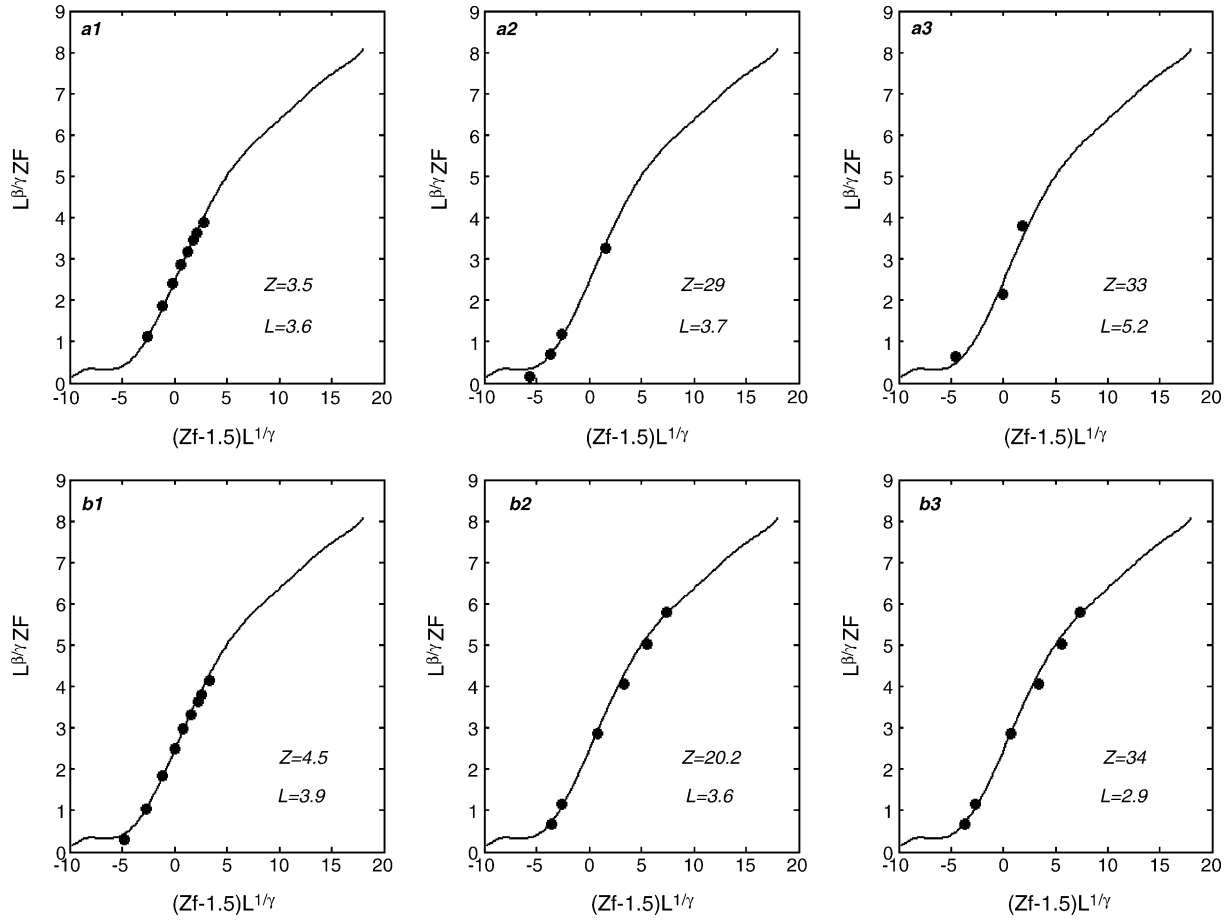

Fig. 8. Fitting process for Z and L of biomorphic Mn oxides, (a1) (a2) (a3) fir template calcined under 600, 800 and 1000 °C, (b1) (b2) (b3) paulownia template calcined under 600, 800 and 1000 °C.

means that the main pore size gets smaller from 2.2 to 2 nm and the broad peak at about 20 nm disappears. The mesopores shrank to nearly micropores due to grain growth. The higher temperature enhances the structural uniformity within the nanoscale of biomorphic Mn oxide, makes the pore size concentrate on 2 nm thus diminishes the average pore diameter, pore volume (expressed as pore numbers) and BET surface area as listed in Table 1.

According to the Fig. 8, the relationship between pore connectivity and calcination temperature is that for the same wood template, the higher the temperature, the better the connectivity is made. The highly interconnected pore channels are derived from the composition and arrangement of various elements (cellulose, hemicellulose, lignin and so on) in the cell wall of tracheid or trachea. The increase of the degree of pore connectivity with the rise of sintering temperature could be attributed to the anisotropic thermal contraction[17] of the skeleton material. Even though the relationship between L and temperature is not evident, but L of each sample is below 10, indicating that even at the beginning stages of desorption, the vaporizing rate of N_2 in pores is relatively high.[26] It suggests that the pores of the biomorphic Mn oxides are highly interconnected with each other and the liquid or gas in the pores could flow with high mobility.

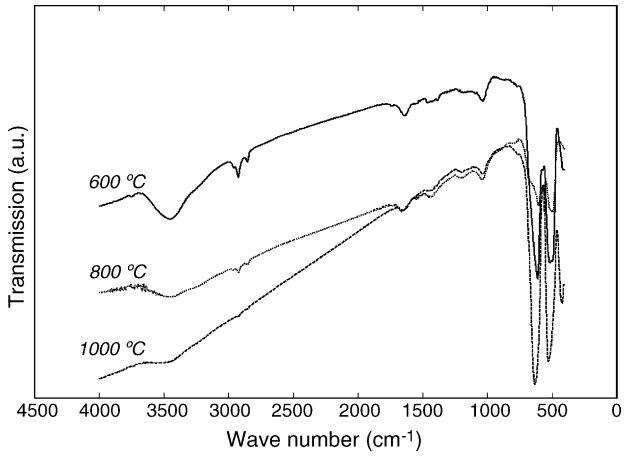

Fig. 9. IR adsorption patterns of fir template biomorphic Mn oxides.

3.3. IR adsorption properties

The IR adsorption patterns of fir template biomorphic Mn oxides calcined at 600, 800 and 1000 °C, respectively, are displayed in Fig. 9.

Apart from the adsorption peaks at 500 and 650 cm^{-1}, which are the characteristic peaks of Mn oxides, it is interestingly found

that the IR spectra exhibit overall collapse beyond 750 cm^{-1} with the rise of calcination temperature. The 1000 °C-calcined biomorphic oxide shows the greatest degree of collapse and slope, therefore the best IR adsorption property. The evolution of pore structure on nanoscale with the rise of calcination temperature as discussed in Section 3.2 may lead to such phenomenon. IR waves enter into nano pore channels causing the sympathetic vibration of cell wall molecules, and therefore, wave energy is dissipated by the vibrations of polar radicals. Then, it could be reasonably deduced that if the pore channels are interconnected with each other to a great extent, more energy dissipation could be resulted in. As discussed in Section 3.2, the pore connectivity of biomorphic Mn oxide increases with the rise of sintering temperature. The 1000 °C-calcined biomorphic Mn oxide possesses the highest degree of pore connectivity, so it shows the best IR adsorption.

The structure-aroused overall collapse of IR spectra could be applied as a function of biomorphic materials with unique pore structure on nanoscale and is worth further studying to obtain more detailed information on the IR adsorption property and its relationship with structure.

4. Conclusion

Porous biomorphic manganese oxides were synthesized on wood template through infiltration with nitrate and then sintering process. The final oxide products contain hierarchical pore structure from micrometer to nanometer scale, and also show unique pore size and distribution even with hierarchy on nanoscale derived from the specific wood template, the changeable connectivity of nano pore channel controlled by calcinations temperature. Depending on the infiltrated wood and the temperature of sintering, the pore structure can be designed. The biodiversity of natural woods offer a variety of different morphologies and composition of cell wall of tracheid or trachea that can be applied in manufacturing biomorphic Mn oxide and even other kind oxides with unique pore structure. The overall collapse in IR adsorption spectra of biomorphic Mn oxides with the rise of calcination temperature is related to the effect of nanoscale pore structure especially the increasing of pore connectivity, and it suggests the good prospect of the use for IR adsorption and even the adsorption of electromagnetic waves of other frequencies of biomorphic materials.

Acknowledgements

The authors wish to express their thanks to the financial support of National Natural Science Foundation of China (No. 50371055), Excellent Young Teachers Program of MOE of China (No. 2062), Key Project on Basic Research of Shanghai (No. 03JC14044), Major Project on Basic research of Shanghai (No. 04DZ14002), Fok Ying Tung Education Fund (No. 94010), Program for New Century Excellent Talents in University (No. NCET-04-0387), Nano-research Program of Shanghai (No. 0452nm045), Research Program of Shanghai (No. 045211059) and National basic research program of China (No. 2006CB601204).

References

1. Tirell, D. A. *et al.*, *Hierarchical Structure in Biology as A Guide for New Materials Technology*. National Academy Press, 1994.
2. Sarikaya, M., Biomimetics: materials fabrication through biology. *PNAS*, 1999, **96**, 14183–14185.
3. Greil, P., Biomorphous ceramics from lignocellulosics. *J. Eur. Ceram. Soc.*, 2001, **21**, 105–118.
4. Greil, P., Lifka, T. and Kaindl, A., Biomorphic cellular silicon carbide ceramics from wood. I. Processing and microstructure. *J. Eur. Ceram. Soc.*, 1998, **18**, 1961–1975.
5. Greil, P., Lifka, T. and Kaindl, A., Biomorphic cellular silicon carbide ceramics from wood. II. Mechanical properties. *J. Eur. Ceram. Soc.*, 1998, **18**, 1975–1983.
6. Ota, T., Takahashi, M., Hibi, T., Ozawa, M., Suzuki, S. and Hikichi, Y., Biomimetic process for producing SiC "wood". *J. Am. Ceram. Soc.*, 1995, **78**, 3409–3411.
7. Vogli, E., Mukerji, J., Hoffmann, C., Kladny, R., Sieber, H. and Greil, P., Conversion of oak to cellular silicon carbide ceramic by gas-phase reaction with silicon monoxide. *J. Am. Ceram. Soc.*, 2001, **84**, 1236–1240.
8. Jumin, Q., Jiping, W. and Zhihao, J., Preparation of biomorphic SiC ceramic by carbothermal reduction of oak wood charcoal. *Mater. Sci. Eng. A*, 2004, **371**, 229–235.
9. Esposito, L., Sciti, D., Piancastelli, A. and Bellosi, A., Microstructure and properties of porous β-SiC templated from soft woods. *J. Eur. Ceram. Soc.*, 2004, **24**, 533–540.
10. Binghe, S., Tongxiang, F., Di, Z. and Okabe, T., The synthesis and microstructure of biomorphic TiC/C ceramics. *Carbon*, 2004, **42**, 177–182.
11. Yongsoon, S., Jun, L., Jeong, H. C., Zimin, N. and Exarhos, G. J., Hierarchically ordered ceramics through surfactant-templated sol-gel mineralization of biological cellular structures. *Adv. Mater.*, 2001, **13**, 728–732.
12. Cao, J., Rambo, C. R. and Sieber, H., Preparation of porous Al_2O_3-ceramics by biotemplating of wood. *J. Porous Mater.*, 2004, **11**, 163–172.
13. Ota, T., Imaeda, M., Takase, H., Kobayashi, M., Kinoshita, N., Hirashita, T., Miyazaki, H. and Hikichi, Y., Porous titania ceramic prepared by mimicking silicified wood. *J. Am. Ceram. Soc.*, 2000, **83**, 1521–1523.
14. Caruso, R. A., Micrometer-to-nanometer replication of hierarchical structures by using a surface sol-gel process. *Angew. Chen. Int. Ed.*, 2004, **43**, 2746–2748.
15. Jianguo, H. and Kunitake, T., Nano-precision replication of natural cellulosic substances by metal oxides. *J. Am. Ceram. Soc.*, 2003, **125**, 11834–11835.
16. Cao, J., Rusina, O. and Sieber, H., Processing of porous TiO_2-ceramics from biological performs. *Ceram. Int.*, 2004, **30**, 1971–1974.
17. Zhaoting L, Tongxiang F, Di Z, Synthesis of biomorphous nickel oxide from pine wood template and investigation on hierarchical pore structure. *J. Am. Ceram. Soc.*, 2006, in press.
18. Zollfrank, C., Kladny, R., Sieber, H. and Greil, P., Biomorphous SiOC/C-ceramic composites from chemically modified wood templates. *J. Eur. Ceram. Soc.*, 2004, **24**, 479–487.
19. Zollfrank, C. and Sieber, H., Microstructure and phase morphology of wood derived biomorphous SiSiC-ceramics. *J. Eur. Ceram. Soc.*, 2004, **24**, 495–506.
20. Rambo, C., Cao, J. and Sieber, H., Preparation and properties of highly porous, biomorphic YSZ-Ceramics. *Mat. Chem. Phys.*, 2004, **87**, 345–352.
21. Eric, S. T. and Ram, S., Spontaneous formation of macroporous monoliths of mesoporous manganese oxide crystals. *Adv. Mater.*, 2005, **17**, 2244–2246.
22. Gibson, L. J., Wood: a natural fibre reinforced composite. *Metals Mater.*, 1992, **8**, 333.
23. Kiyotaka, S., Yoshihiro, O., Takayuki, O., Masahiro, S., Akira, Y. and Ryoichi, Y., Electromagnetic shielding properties of woodceramics made from wastepaper. *J. Porous Mater.*, 1997, **4**, 269–275.
24. Seaton, N. A., Walton, J. and Quirke, N., A new analysis method for the determination of the pore size distribution of porous carbons from nitrogen adsorption measurements. *Carbon*, 1989, **27**, 853–861.

25. Seaton, N. A., Determination of the connectivity of porous solids from nitrogen sorption measurements. *Chem. Eng. Sci.*, 1991, **46**, 1895–1909.
26. Seaton, N. A. and Hailing, L., Determination of the connectivity of porous solids from nitrogen sorption measurements. *Chem. Eng. Sci.*, 1994, **49**, 1869–1878.
27. Singh, M. and Yee, B.-M., Reactive processing of environmentally conscious, biomorphic ceramic from natural wood precursors. *J. Eur. Ceram. Soc.*, 2004, **24**, 209–217.
28. Angang, D., Yajun, W., Yi, T., Nan, R., Yahong, Z., Yinghong, Y. and Zi, G., Zeolitic tissue through wood cell templating. *Adv. Mater.*, 2002, **14**, 926–929.
29. Greil, P., Vogli, E., Fey, T., Bezold, A., Popovska, N., Gerhard, H. and Sieber, H., Effect of microstructure on the fracture behavior of biomorphous silicon carbide ceramics. *J. Eur. Ceram. Soc.*, 2002, **22**, 2697–2707.
30. Davis, S. A., Burkett, S. L., Mendelson, N. H. and Mann, S., Bacterial templating of ordered macrostructures in silica and silica-surfactant mesophases. *Nature*, 1997, **385**, 420–423.